Programmable mode conversion and bandgap formation for surface acoustic waves using piezoelectric metamaterials

Salih Alan, Ahmed Allam, and Alper Erturk[a)]
G. W. Woodruff School of Mechanical Engineering, Georgia Institute of Technology, Atlanta, Georgia 30332, USA

(Dated: 18 August 2019)

A spatially reversible and programmable piezoelectric metamaterial concept is introduced for the manipulation of surface acoustic waves to achieve on-demand wave mode conversion and reflection. The concept uses an array of inductive-shunted piezoelectric elements (with gradually varying inductors in space) attached to the surface of an elastic propagation domain. The value of each inductor directly controls the phase velocity of the Rayleigh wave locally as quantified through unit cell band diagram analysis that guides the design process. By varying the spatial inductance distribution, the proposed piezoelectric metamaterial domain can be programmed to convert incident surface waves into bulk shear waves or reflect them completely. The location of surface-to-bulk wave mode conversion or wave reflection can be tailored by means of the inductance distribution, and the directional behavior in space can be reversed. The proposed concept may enable novel surface acoustic wave devices and filters, via digital or analog programmable shunt circuits.

Metamaterial and phononic crystal concepts have been explored by numerous research groups to manipulate the propagation of different types of elastic waves, including Rayleigh[1–3], Love[4,5], and Lamb[6–8] waves. Through the careful design of these engineered materials, wave propagation characteristics can be tailored with capabilities spanning from bandgap formation[2,3,9–12] to wave focusing[7,8,13,14], among others. These design concepts have also been applied to large scale problems such as seismic and vibration isolation[15–17] as well as small scale applications in surface acoustic wave (SAW) devices[9,18–20].

Bandgap formation for elastic/acoustic waves can be achieved via phononic crystals[21,22] or locally resonant inclusions[23–25], and in some cases using both approaches[26,27]. Several structures have been proposed to manipulate surface waves, such as periodic holes[3,9,10,12,28], hard cylinders or spheres buried in a softer background near the surface[29,30], resonant pillars, rods or stubs mounted on the free surface[11,17,26,31,32], and buried resonators[15,16]. The inclusion properties can also be varied gradually to achieve a spatial change in the effective material properties for surface wave steering[14,33]. Gradient-index metamaterials have been also used to convert Rayleigh waves into bulk waves. Colombi et al.[17,32] proposed a resonant metawedge by placing trees on the ground with gradually increasing heights, which correspond to decreasing their resonance frequencies and therefore the formation of attenuation bands at lower frequencies. The resonant metawedge was able to reflect Rayleigh waves arriving from the side of shorter trees, while it was able to convert these waves into bulk waves if they arrived from the side of taller trees. Later they experimentally validated this concept using a small scale model for ultrasonic frequencies[34].

[a)]Electronic mail: alper.erturk@me.gatech.edu; author to whom correspondence should be addressed

In parallel to these efforts, several methods have been explored to tune surface wave propagation characteristics of metamaterials. This includes using temperature control to actively steer and focus surface waves[35], acoustoelectric interactions to tune defect modes for filtering applications[36], and magnetic modulation to tune contact resonances of metallic beads[37]. The aforementioned tree-based metawedge concept for wave mode conversion and bandgap formation can be scaled down and made programmable for SAW applications, and piezoelectric materials are well suited for that purpose. In the following, we explore piezoelectric-based implementation of wave mode conversion in a programmable domain with simple circuitry, which may offer new opportunities in surface wave control and redirection.

The programmable metamaterial domain proposed in this work consists of an array of piezoelectric elements (unit cells) mounted on a homogeneous elastic substrate as shown in Fig. 1a. Each piezoelectric element is shunted to an inductor that shapes the dynamics (i.e. dispersion behavior) of the respective unit cell in the frequency neighborhood of interest. This structure can be programmed to let the incident surface wave propagate uninterrupted, convert them to shear waves (Fig. 1b) or reflect them completely (Fig. 1c).

Spatial distribution of inductance values for the type of wave redirection (e.g. mode conversion or reflection) is based on a unit cell band diagram analysis. In the specific case study of this work (that is focused on concept demonstration with representative results), each unit cell (Fig. 1a) consists of a piezoelectric element of height $h_r = 2\,\text{mm}$, thickness $t_r = 1.5\,\text{mm}$, width $w_r = 72\,\text{mm}$, and is made of a piezoelectric material with surface electrodes perpendicular to the poling direction as shown in the figure. PZT-5H is used here as a commonly available option. The resonators are attached onto a homogeneous and isotropic elastic wave propagation domain, i.e. substrate (aluminum in this work). The resonator periodicity in the direction of wave propagation

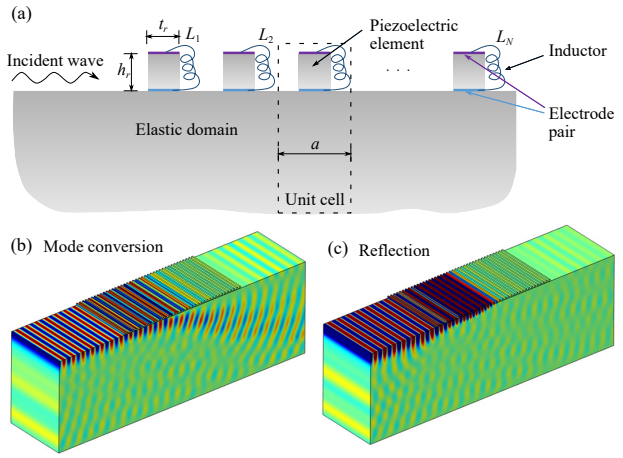

FIG. 1. (a) Schematic of an inductive shunted piezoelectric array (with gradually varying inductance values) for two programmable and spatially reversible concepts: (b) mode conversion and (c) reflection of Rayleigh waves.

is $a = 3.6\,\text{mm}$. The band diagram for a piezoelectric element (with its surface electrodes shorted) and sufficiently deep aluminum domain is plotted in Fig. 2a. The diagram was obtained by constructing a piezoelectric-elastic finite element model of the unit cell shown in Fig. 1a coupled with the electrical circuit module using COMSOL Multiphysics. The dashed lines indicate Rayleigh, shear, and pressure waves of the homogeneous substrate away from the metamaterial. The shear wave line of the substrate divides the band diagram into two regions: the bulk wave domain which corresponds to the region above the shear wave line and the surface wave domain below the shear wave line. The presence of the periodic piezoelectric elements at the surface of the substrate introduces a surface wave bandgap around a select target (design) frequency. The range of the bandgap frequency is determined by the geometry of the piezoelectric elements. Importantly, by connecting an inductor across the surface electrodes of the piezoelectric unit cell, a propagation mode can be introduced inside this bandgap as shown in Fig. 2b. For a target frequency f (in Hz) in this propagation band, the phase velocity c of the resulting surface wave is

$$c = \frac{2\pi f}{k}, \tag{1}$$

where k is the wavenumber. The propagation mode frequency range is roughly controlled by the relation:

$$f_e = \frac{1}{2\pi\sqrt{LC_p}}, \tag{2}$$

where L is the shunt inductance, C_p is the capacitance of the piezoelectric element, and f_e is the electrical resonance frequency. The estimated value from Eq. (2) is useful for an analytical insight and is approximate due to the two-way electromechanical coupling between the electrical circuit, piezoelectric element, and substrate.[38] As can be expected, a higher value of inductance results in lower electrical resonance, which shifts the propagation band accordingly as shown in Fig. 3a. This results in a lower surface wave phase velocity as the intersection between the horizontal target frequency line and the propagation band happens at a higher wavenumber (here, 250 kHz is used as the target frequency). At the target frequency, the relationship between the phase velocity and the inductance value is shown in Fig. 3b. For the investigated configuration, surface wave propagation is only possible for inductance values between 0.24 mH - 0.44 mH. The surface wave phase velocity matches the Rayleigh wave velocity of the substrate for a 0.275 mH inductor. Starting from this value and decreasing the inductance increases the surface wave phase velocity up to the value of shear wave velocity, yielding the conversion of incident surface waves into shear waves propagating into the substrate. On the other hand, starting with the same inductor and increasing the value of the inductance reduces the surface wave velocity until the wave enters the bandgap and a total reflection is observed. These are the two fundamental mechanisms to program the unit cells of the proposed metamaterial domain for wave mode conversion and reflection at a desired position in space.

The aforementioned substantial control over the effective surface wave velocity for a unit cell enables strong manipulation of surface waves incident to an array of these cells that forms the programmable metamaterial domain. In order demonstrate this, we consider an array of 40 piezoelectric elements with identical geometry. The phase velocity for the first element in the array is set to match the Rayleigh wave velocity of the substrate ($c_R = 2907\,\text{m/s}$) so that impedance mismatch is minimized. The array can then be programmed to achieve mode conversion by gradually changing the inductance value between each two consecutive elements to increase the wave speed up to the shear wave speed. The spatial position at which this conversion takes place is controlled by the inductance distribution. Fig. 4a shows RMS (root mean square) wavefields for three different inductance distribution cases which are displayed in Fig. 4b. Rayleigh waves are incident from the left side of the device and low reflecting boundary conditions are used to minimize the reflections at the boundaries of the elastic domain. As can be observed clearly, the proposed concept not only achieves mode conversion but also provides an authority to control its location.

The position of wave mode conversion is mainly controlled by the position of the unit cell (piezoelectric element) whose inductance value is such that the wave speed matches the shear wave speed of the substrate. By shifting this match spatially in Cases 1a, 1b, and 1c, the location of mode conversion is accurately controlled. It is useful to note that for all three cases in Fig. 4a, shear waves exhibit an angle of approximately 69° from the vertical direction (angle of refraction), following Snell's law between the incident and refracted wave speeds, which

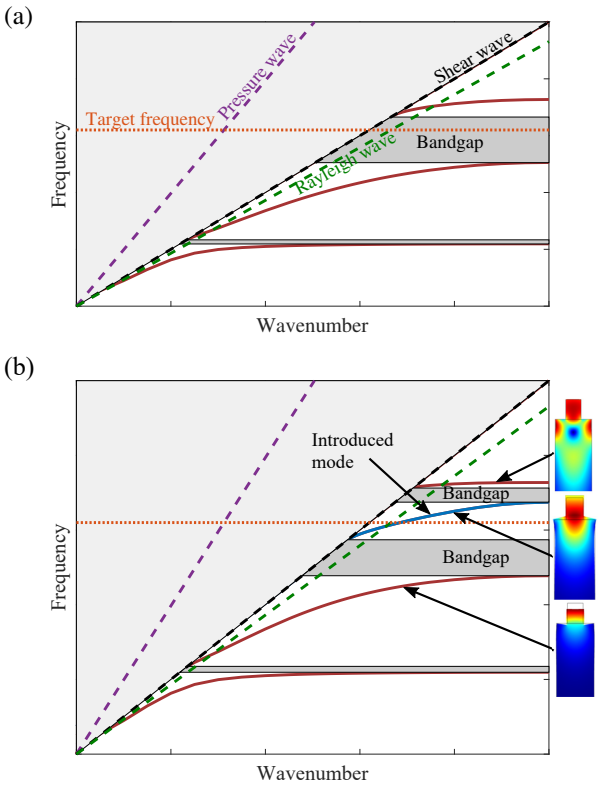

FIG. 2. Representative cases of the band diagrams for (a) short-circuit and (b) inductive-shunted cases. Piezoelectric element geometry is designed to have a Rayleigh wave bandgap around the target frequency. Inductive shunt divides the bandgap into two and introduces a propagation band in between (mode shapes are shown as insets).

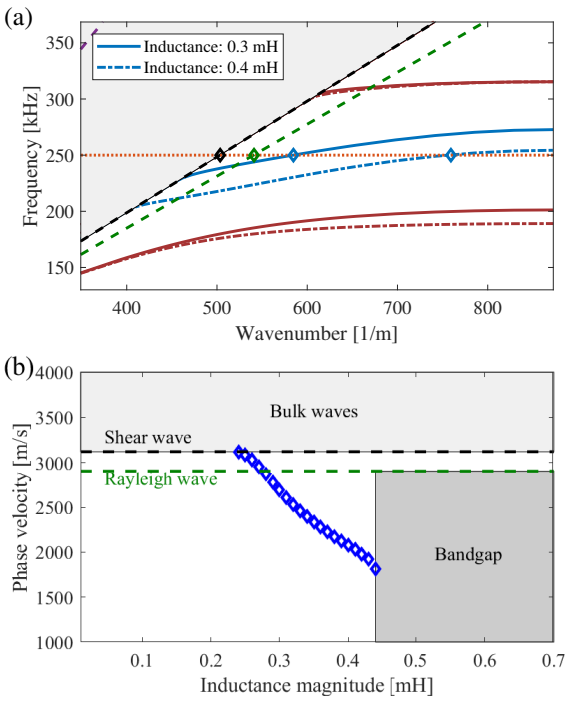

FIG. 3. (a) Band diagram for inductive-shunted unit cells with two different inductance values. Intersection of the horizontal line at target frequency (250 kHz) with the shear wave and Rayleigh wave lines and the inductive shunt propagation band are shown. (b) Phase velocity vs. inductance at the target frequency (250 kHz). An inductance range of 0.01 mH - 0.7 mH is shown. No data range means no intersection in the surface wave region which indicates the presence of a bandgap.

are, respectively, the Rayleigh and shear wave speeds.

A similar spatial control can be achieved for reflecting incident surface waves (at the same frequency) as shown in Fig. 5 by reprogramming the metamaterial domain, i.e. by modifying the inductance distribution. The exact position of the reflection is determined by the position of the unit cell at which the bandgap starts. As can be observed in Fig. 5b, this match is around 5^{th} element in Case 2a, 15^{th} element in Case 2b, and 25^{th} element in Case 2c. Therefore, it is possible to modify the proposed piezoelectric metamaterial domain for both wave mode conversion and reflection. It is also possible to easily reverse the spatial propagation direction for both purposes.

It is worth mentioning that, just like in the purely mechanical counterpart of the problem[16], it is possible to achieve wave mode conversion with identical resonators (i.e. with identical piezoelectric unit cells of identical inductors) as shown in Fig. 6. However, this configuration results in an increased reflection due to the sudden transition of the wave into the metamaterial domain rather than the gradual one achieved using varying inductors (cf. Figs. 4 and 6 - the color scale is the same). Finally, the number of resonators was chosen to be relatively high in this work merely to show the capability of the spatial position control over mode conversion and reflection in Figs. 4 and 5, respectively. It is possible to realize the resulting behavior with less number of resonators as shown in Fig. 7 for mode conversion (which applies to bandgap-based reflection as well). In a given application, therefore, to minimize fabrication effort and complexity, one might reduce the number of resonators if the spatial resolution to control wave mode conversion or reflection does not have to be very fine. Below a certain number of resonators, however, the relevant phenomenon (mode conversion or reflection) would cease to exist as observed in locally resonant metamaterials and metastructures[25,39]. Note that, in Fig. 7, some of the surface wave energy is already transmitted (leaked) to the other side of the metamaterial domain in case of 10 resonators, and this leakage increases with reduced number of resonators.

To conclude, a programmable piezoelectric metamaterial capable of redirecting incident surface acoustic waves is introduced and demonstrated via case studies. Conversion of surface waves into shear waves and reflection of surface waves are demonstrated in detail. The metamaterial domain can be reprogrammed not only to switch between these tasks (which can also be spatially reversed)

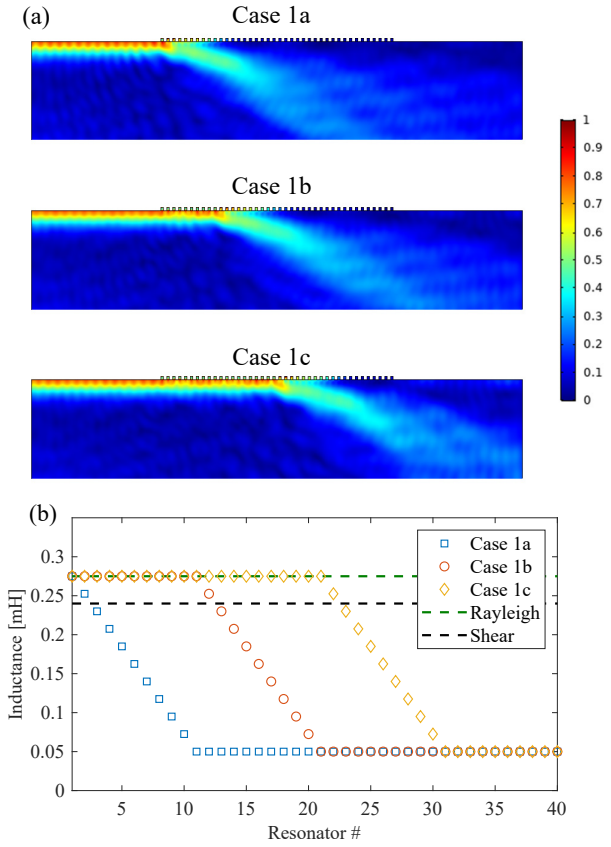

FIG. 4. (a) Conversion of Rayleigh waves into shear waves (RMS wavefields are shown) and (b) associated inductance distribution to achieve mode conversion at three distinct positions (at 250 kHz). In each case, mode conversion starts where the shear line is crossed. See the multimedia animation for a specific instance (Case 1b). (Multimedia view)

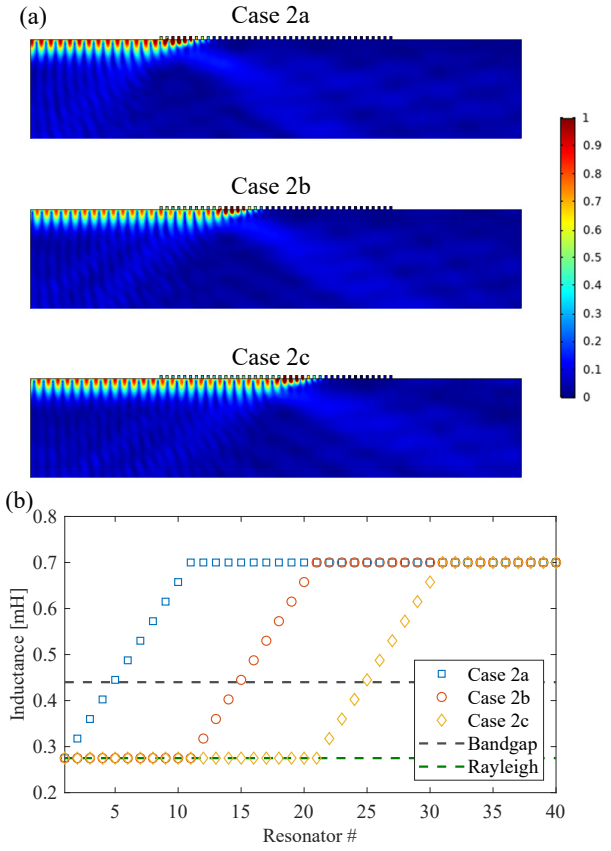

FIG. 5. (a) Reflection of Rayleigh waves (RMS wavefields are shown) and (b) associated inductance distribution to achieve reflection via bandgap formation at three distinct positions (at 250 kHz). In each case, reflection starts where the bandgap line is crossed. See the multimedia animation for a specific instance (Case 2b). (Multimedia view)

but also to accurately specify the spatial position (of mode conversion or reflection). This fine control on surface wave propagation through simple circuitry may enable opportunities in electromechanical devices based on surface waves (SAW filters, etc.) and other small scale configurations that could benefit from tunable and programmable modality. While the current paper is centered on the demonstration of the proposed concept and its basic characteristics, future efforts may explore higher frequency implementation and small scale (MEMS) fabrication of such miniaturized devices with integrated circuits for potential SAW applications[40], among others.

S.A. acknowledges international postdoctoral research scholarship (program 2219) from the Scientific and Technological Research Council of Turkey (TUBITAK). A.A. and A.E. acknowledge support from the U.S. National Science Foundation CMMI Grant 1727951.

[1]Y. Tanaka and S.-i. Tamura, Phys. Rev. B **58**, 7958 (1998).
[2]T.-T. Wu, Z.-C. Hsu, and Z.-G. Huang, Phys. Rev. B **71**, 064303 (2005).
[3]V. Laude, M. Wilm, S. Benchabane, and A. Khelif, Phys. Rev. E **71**, 036607 (2005).
[4]T.-W. Liu, Y.-C. Lin, Y.-C. Tsai, T. Ono, S. Tanaka, and T.-T. Wu, Appl. Phys. Lett. **104**, 181905 (2014).
[5]T.-W. Liu, Y.-C. Tsai, Y.-C. Lin, T. Ono, S. Tanaka, and T.-T. Wu, AIP Advances **4**, 124201 (2014).
[6]Y. Jin, D. Torrent, Y. Pennec, Y. Pan, and B. Djafari-Rouhani, Journal of Applied Physics **117**, 244904 (2015).
[7]S. Tol, F. L. Degertekin, and A. Erturk, Appl. Phys. Lett. **109**, 063902 (2016).
[8]S. Tol, F. L. Degertekin, and A. Erturk, Appl. Phys. Lett. **111**, 013503 (2017).
[9]T.-T. Wu, L.-C. Wu, and Z.-G. Huang, Journal of Applied Physics **97**, 094916 (2005).
[10]S. Benchabane, A. Khelif, J.-Y. Rauch, L. Robert, and V. Laude, Phys. Rev. E **73**, 065601 (2006).
[11]A. Khelif, Y. Achaoui, S. Benchabane, V. Laude, and B. Aoubiza, Phys. Rev. B **81**, 214303 (2010).
[12]D. Yudistira, Y. Pennec, B. Djafari Rouhani, S. Dupont, and V. Laude, Appl. Phys. Lett. **100**, 061912 (2012).
[13]M. Addouche, M. A. Al-Lethawe, A. Choujaa, and A. Khelif, Appl. Phys. Lett. **105**, 023501 (2014).
[14]J. Zhao, B. Bonello, L. Becerra, O. Boyko, and R. Marchal, Appl. Phys. Lett. **108**, 221905 (2016).
[15]S. Krödel, N. Thomé, and C. Daraio, Extreme Mechanics Letters **4**, 111 (2015).
[16]A. Palermo, S. Krödel, A. Marzani, and C. Daraio, Scientific Reports **6**, 39356 (2016).
[17]A. Colombi, D. Colquitt, P. Roux, S. Guenneau, and R. V.

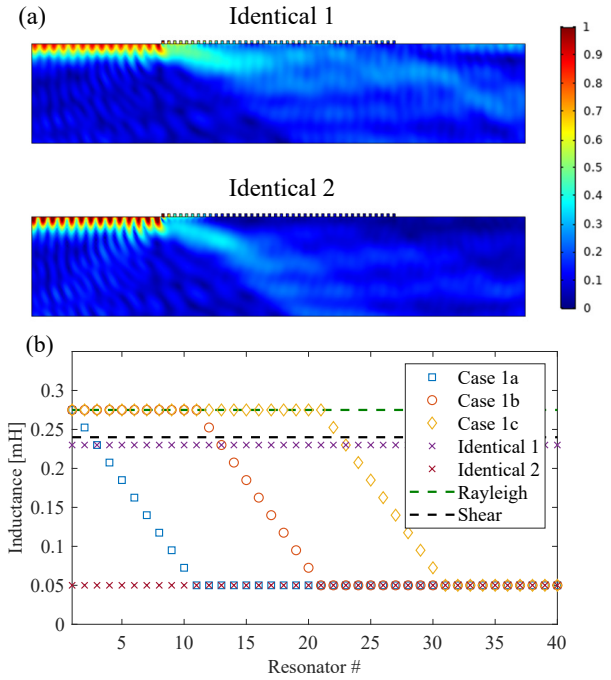

FIG. 6. (a) Wave mode conversion (RMS wavefield) for two cases of identical resonators revealing increased reflection due to abrupt transition rather than the gradual transition previously demonstrated in FIG. 4 and (b) associated inductance distribution in comparison to previous cases (250 kHz).

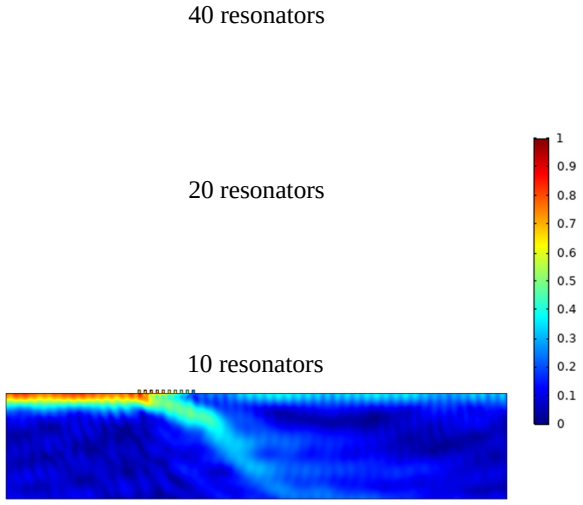

FIG. 7. Wave mode conversion for different number of resonators, including the case with 40 resonators as Case 1a in Fig. 4a, which was preferred to clearly show the spatial control over wave mode conversion (RMS wavefield at 250 kHz).

Craster, Scientific Reports **6**, 27717 (2016).

[18] D. A. Fuhrmann, S. M. Thon, H. Kim, D. Bouwmeester, P. M. Petroff, A. Wixforth, and H. J. Krenner, Nature Photonics **5**, 605 (2011).

[19] V. Yantchev, Appl. Phys. Lett. **104**, 103503 (2014).

[20] D. Yudistira, A. Boes, B. Graczykowski, F. Alzina, L. Y. Yeo, C. M. Sotomayor Torres, and A. Mitchell, Phys. Rev. B **94**, 094304 (2016).

[21] M. S. Kushwaha, P. Halevi, L. Dobrzynski, and B. Djafari-Rouhani, Physical review letters **71**, 2022 (1993).

[22] J. Vasseur, P. A. Deymier, B. Chenni, B. Djafari-Rouhani, L. Dobrzynski, and D. Prevost, Physical Review Letters **86**, 3012 (2001).

[23] Z. Liu, X. Zhang, Y. Mao, Y. Zhu, Z. Yang, C. T. Chan, and P. Sheng, science **289**, 1734 (2000).

[24] M. Nouh, O. Aldraihem, and A. Baz, Journal of Sound and Vibration **341**, 53 (2015).

[25] C. Sugino, S. Leadenham, M. Ruzzene, and A. Erturk, Journal of Applied Physics **120**, 134501 (2016).

[26] Y. Achaoui, A. Khelif, S. Benchabane, L. Robert, and V. Laude, Phys. Rev. B **83**, 104201 (2011).

[27] L. Liu and M. I. Hussein, Journal of Applied Mechanics **79**, 011003 (2012).

[28] S. Brûlé, E. H. Javelaud, S. Enoch, and S. Guenneau, Phys. Rev. Lett. **112**, 133901 (2014).

[29] J.-H. Sun and T.-T. Wu, Phys. Rev. B **74**, 174305 (2006).

[30] R. Sainidou, B. Djafari-Rouhani, and J. O. Vasseur, Phys. Rev. B **77**, 094304 (2008).

[31] A. Khelif, Y. Achaoui, and B. Aoubiza, AIP Advances **1**, 041404 (2011).

[32] A. Colombi, R. V. Craster, D. Colquitt, Y. Achaoui, S. Guenneau, P. Roux, and M. Rupin, Front. Mech. Eng. **3**, 10 (2017).

[33] A. Palermo and A. Marzani, Scientific Reports **8**, 7234 (2018).

[34] A. Colombi, V. Ageeva, R. J. Smith, A. Clare, R. Patel, M. Clark, D. Colquitt, P. Roux, S. Guenneau, and R. V. Craster, Scientific Reports **7**, 6750 (2017).

[35] N. Cselyuszka, M. Seujski, N. Engheta, and V. Crnojevi-Bengin, New J. Phys. **18**, 103006 (2016).

[36] F. Taleb and S. Darbari, Phys. Rev. Applied **11**, 024030 (2019).

[37] A. Palermo, Y. Wang, P. Celli, and C. Daraio, Phys. Rev. Applied **11**, 044057 (2019).

[38] N. W. Hagood and A. von Flotow, Journal of Sound and Vibration **146**, 243 (1991).

[39] C. Sugino, S. Leadenham, M. Ruzzene, and A. Erturk, Smart Mater. Struct. **26**, 055029 (2017).

[40] C. Campbell, *Surface Acoustic Wave Devices and Their Signal Processing Applications* (Academic Press, 2012).